Estimating the Column Density in Molecular Clouds with Far-Infrared and Submillimeter Emission Maps

The Astrophysical Journal, 640: L47–L50, 2006 March 20

ESTIMATING THE COLUMN DENSITY IN MOLECULAR CLOUDS WITH FAR-INFRARED AND SUBMILLIMETER EMISSION MAPS

S. Schnee,[1] T. Bethell,[2] and A. Goodman[1]

Received 2005 November 8; accepted 2006 February 9; published 2006 March 2

ABSTRACT

We have used a numerical simulation of a turbulent cloud to synthesize maps of the thermal emission from dust at a variety of far-IR and submillimeter wavelengths. The average column density and external radiation field in the simulation is well matched to clouds such as Perseus and Ophiuchus. We use pairs of single-wavelength emission maps to derive the dust color temperature and column density, and we compare the derived column densities with the true column density. We demonstrate that longer wavelength emission maps yield less biased estimates of column density than maps made toward the peak of the dust emission spectrum. We compare the scatter in the derived column density with the observed scatter in Perseus and Ophiuchus. We find that while in Perseus all of the observed scatter in the emission-derived versus the extinction-derived column density can be attributed to the flawed assumption of isothermal dust along each line of sight, in Ophiuchus there is additional scatter above what can be explained by the isothermal assumption. Our results imply that variations in dust emission properties within a molecular cloud are not necessarily a major source of uncertainty in column density measurements.

Subject headings: dust, extinction — ISM: clouds — surveys

Online material: color figures

1. INTRODUCTION

In the absence of direct measurements of extinction, the column density of dust in molecular clouds is often traced by dust emission. In many cases, the data are maps at two wavelengths in the far-infrared (FIR) or submillimeter, and the column density is derived by assuming that dust along each line of sight is isothermal (Wood et al. 1994; Schlegel et al. 1998; Schnee et al. 2005). However, each line of sight through a molecular cloud is likely to intersect regions with various amounts of shielding, and therefore a range of temperatures, so the isothermal assumption may lead to significant errors in the calculation of column density.

In this Letter we use a simulation of an externally heated turbulent molecular cloud to produce maps of column density and thermal emission at various FIR and submillimeter wavelengths. We discuss the bias in the emission-derived column density as a function of extinction and wavelength, and we compare the scatter in the emission-based column density estimate with that observed in Schnee et al. (2005) in the Perseus and Ophiuchus molecular clouds. We find that assuming isothermality can account for all of the observed point-by-point scatter in comparisons of extinction- and emission-based column density maps of Perseus without the need to invoke variations in the dust properties within a molecular cloud or variations in the emission from stochastically heated grains. In comparison, the scatter in Ophiuchus is significantly larger than can be accounted for by the error introduced by the isothermal dust assumption alone.

2. THE MODEL CLOUD

The methods for determining the dust distribution, radiative transfer, and dust heating, only briefly described in this section, are described in more detail in Bethell et al. (2004).

[1] Harvard-Smithsonian Center for Astrophysics, 60 Garden Street, Cambridge, MA 02138; sschnee@cfa.harvard.edu.

[2] Department of Astronomy, University of Wisconsin at Madison, 5534 Sterling Hall, 475 North Charter Street, Madison, WI 53706.

2.1. *Density Structure*

The density structure is created by a three-dimensional simulation of driven MHD turbulence on a cubical grid with 128 cells on a side (Heitsch et al. 2001). Although the original ensemble of simulations was created with widely varying physical parameters (Mach number, plasma beta, etc.), the radiative transfer through the resulting structures is largely insensitive to these differences. To simulate Perseus and Ophiuchus, we use one such model and scale the density and size of our model cloud so that the column density map has an average $A_V \sim 2$, which is the median A_V in our Perseus and Ophiuchus extinction maps. This choice of model is meant to be illustrative of the broad effects of including "realistic" clumpiness in radiative transfer calculations of molecular clouds. When compared to a uniform density distribution of similar mass, the inclusion of clumpiness tends to expose more of the *volume* to the interstellar radiation field (ISRF) while, on average, the *mass* is both less illuminated and illuminated by bluer light. In the clumpy case, there is also little correlation between the intracloud radiation field at a point and its proximity to the cloud edge. Instead, there is a large point-to-point scatter, arising from the details of the clumpiness (Bethell et al. 2004).

2.2. *Radiative Transfer*

A reverse Monte Carlo radiative transfer code (Bethell et al. 2004) is used to calculate the penetration of an external isotropic and homogeneous ISRF; here the ISRF is given by Mathis et al. (1983). The reverse Monte Carlo technique enables the user to control the Monte Carlo photon noise in regions that are well shielded, in particular, the clumps where most of the mass resides. The reemission by dust of submillimeter radiation is assumed to be optically thin throughout our cloud.

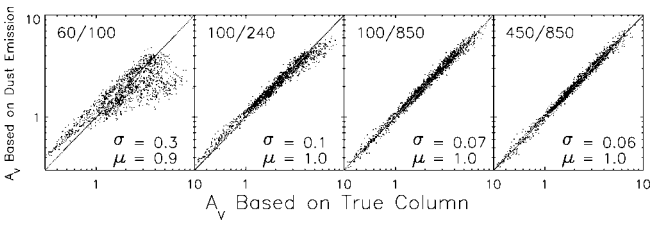

FIG. 1.—Column density derived from two emission maps plotted against the true column density. The wavelengths used are, *from left to right*, 60 and 100 μm, 100 and 240 μm, 100 and 850 μm, and 450 and 850 μm. The values of X that convert from the FIR optical depth to visual extinction are $\tau_{100} = 775$, $\tau_{100} = 231$, $\tau_{100} = 69$, and $\tau_{450} = 681$. The values of μ and σ refer to the center and width of the Gaussian fit to the distribution of the ratio ($A_{V_{\rm emission}}/A_{V_{\rm true}}$). [*See the electronic edition of the Journal for a color version of this figure.*]

2.3. *Dust Properties*

To calculate self-consistently the attenuation of the ISRF by dust, the subsequent equilibrium dust temperature, and the FIR emission, we use astronomical silicate and graphite grain opacities (Draine & Lee 1984)[3] and a power-law grain size distribution (Mathis et al. 1977). These are chosen to reproduce an extinction curve with $R_V = A_V/E(B-V) = 3.1$. No attempt is made to include very small grains that are heated transiently to high temperatures, nor do we include polycyclic aromatic hydrocarbon emission. Both these populations contribute significantly to wavelengths shorter than 100 μm.

At far-infrared wavelengths ($\lambda > 100$ μm), the dust ensemble emission is described by a blackbody spectrum modified by a power law [$S_\lambda \propto B_\lambda(T_d)\lambda^{-\beta}$] with an emissivity spectral index of $\beta = 2$. With the dust ensemble fully prescribed, we can calculate the equilibrium grain temperatures of each grain type and grain size at each location. Not only do dust temperatures vary along each line of sight, they also vary among grain types and sizes at any point within the cloud.

3. DERIVED COLOR TEMPERATURE AND COLUMN DENSITY

The method used to determine the dust temperature and column density from two emission maps is similar to that used in Schnee et al. (2005). The dust temperature (T_d) is determined by the ratio of two flux densities, and the column density can be derived from either flux and the derived color temperature of the dust. The pairs of fluxes that we study in this Letter are 60 and 100 μm (the longest wavelength *IRAS* bands), 100 and 240 μm (those used in Schlegel et al. 1998, hereafter SFD98), 100 and 850 μm, and 450 and 850 μm (wavelengths observed by SCUBA on the James Clerk Maxwell Telescope; Holland et al. 1999).

To determine the dust color temperature, we use the equation

$$R = \left(\frac{\lambda_1}{\lambda_2}\right)^{-(5+\beta)} \left[\frac{\exp\left(hc/\lambda_2 kT_d\right) - 1}{\exp\left(hc/\lambda_1 kT_d\right) - 1}\right], \quad (1)$$

where R is the ratio of the fluxes and β is the emissivity spectral index of the dust. We calculate the dust temperature with the assumption that $\beta = 2$, which is true of the dust in our model. Note that in using the ratio of two flux maps to get the color temperature, we are assuming that a single temperature, T_d, can be used to describe all the dust along each line of sight.

The optical depth is determined by the ratio of the flux to the Planck function:

$$\tau_\lambda = \frac{F_\lambda}{B_\lambda(T_d)}, \quad (2)$$

with the assumption that the dust emission is optically thin.

The optical depth can then be converted to V-band extinction using

$$A_V = X\tau_\lambda, \quad (3)$$

where X is a parameter relating the thermal emission properties of dust to its optical absorption qualities. The extinction, A_V, is derived from the column density of dust in our model, using the conversions $N_{\rm H}/E(B-V) = 5.8 \times 10^{21}$ cm^{-2} and $A_V/E(B-V) = 3.1$. We use the IDL procedure AMOEBA to determine the value of X that minimizes the difference between the emission-derived column density and the true column density in the simulation.

4. RESULTS

4.1. *Dependence on Wavelength*

The column density of dust derived from pairs of thermal emission maps depends strongly on the two wavelengths considered. Figure 1 shows that the 60 and 100 μm derived column density is a linear tracer of the actual column density for $A_V < 1$ mag, but it systematically underestimates the true column density for $A_V > 1$ mag. The same trend is seen in the column density derived from the 100 and 240 μm emission maps, although the cutoff extinction above which the column densities are underestimated is $A_V \sim 4$ mag. The column density derived from the 100 and 850 μm maps traces the true column density all the way to $A_V = 10$ mag, as does the column density derived from the 450 and 850 μm emission maps. The errors introduced by the assumption of isothermal dust along each line of sight for each pair of maps is shown in Figure 1.

The underestimation of column density at $A_V > 1$ as derived from the 60 and 100 μm emission maps comes from an overestimate of dust temperature along lines of sight that pass through various environments with different temperatures. The emission is then dominated by the warmer regions, while the column density is dominated by the cooler and denser regions. The derived color temperature is thus more representative of the warmer regions, and the derived optical depth is therefore too low. This effect can be seen clearly in the leftmost panel of Figure 1. Because X has been scaled to minimize the difference between the emission- and absorption-derived column densities, the derived column densities of points below $A_V = 1$ are overestimated. This problem is much less significant when the emission maps are in the Rayleigh-Jeans portion of the dust emission spectrum (Bethell et al. 2004), which explains why the two panels on the right side of Figure 1 show a much tighter correlation between the derived column density and the true column density than the two panels on the left. Similarly, the longer wavelength emission maps, shown in Figure 2, trace the true column density much better than the shorter wavelength maps.

[3] For tabulated optical properties, visit the Web site http://www.astro.princeton.edu/~draine.

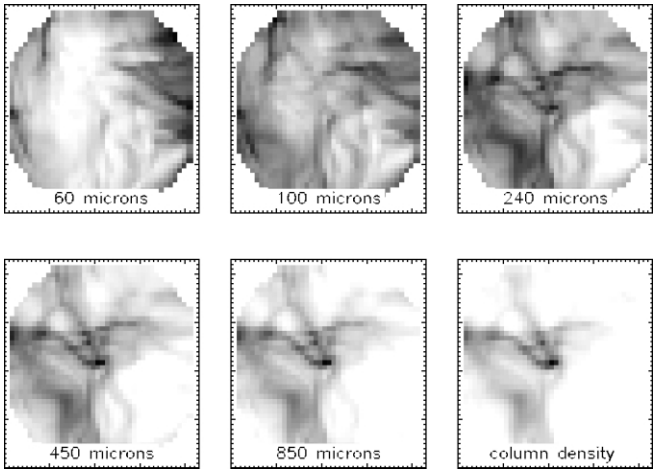

FIG. 2.—Flux maps at the five wavelengths considered in the Letter, plotted along with the true column density. All of the maps are scaled to have the same dynamic range, with their maxima black and minima white.

4.2. *Variable Dust Properties*

In order to isolate the effect of the assumption of isothermal dust along each line of sight through a molecular cloud on the emission-derived column density, we have kept the dust properties in our model invariant. However, recent observations have shown that the overall submillimeter emissivity of dust grains varies within a molecular cloud (Stepnik et al. 2003) and that the emissivity spectral index of dust within a molecular cloud also varies (Dupac et al. 2003). The scatter between the emission-derived column density and the true column density shown in Figure 1 arises solely from the assumption of isothermal dust and does not include the effects of variable dust emission properties. When the column density is derived from 60 and 100 μm observations, the effect of variable grain properties may not be important, because the assumption of isothermal dust makes deriving the column density from emission maps impractical above $A_V > 1$ while dust properties are not seen to vary significantly below $A_V < 2$ (Stepnik et al. 2003). When the emission maps are longer wavelength (e.g., from DIRBE, PRONAOS, or SCUBA), the assumption of isothermal dust is less problematic (as shown in Fig. 1), and the variable dust properties may become the dominant source of error in the emission-derived column density.

4.3. *Emission from Very Small Grains*

We have shown in Schnee et al. (2005) that the 60 μm emission of molecular clouds comes predominantly from transiently heated, very small dust grains (VSGs). In order to derive the dust temperature, we have removed the VSG contribution to the 60 μm IRAS flux. Because we have no way to determine the VSG contribution on a pixel-by-pixel basis, we assume that the percent emission from VSGs at 60 μm is constant everywhere in Perseus and Ophiuchus. We then determine the 60 μm scale factor such that the median temperature in our maps is equal to the median temperature derived by SFD98 for the same area. The SFD98 temperature maps were derived using 100 and 240 μm data and are therefore unbiased by the emission from the VSGs. This procedure is identical to that performed in Schnee et al. (2005). The 60 μm flux from our model was not subjected to such a scaling factor because no VSG contribution to the flux was included.

Although scaling the 60 μm flux by a constant multiplicative factor can give the proper *average* temperature, each line of sight through our observed molecular clouds should ideally be treated with its own scaling factor. The variable VSG contribution to the 60 μm flux cannot be removed on a pixel-by-pixel basis because the SFD98 resolution is too coarse, and this introduces errors in the derivation of dust temperature and column density. Applying a constant scale factor to the 60 μm flux does not correct for this error nor does it introduce additional scatter in Figure 3. The derived value of X does depend on this scale factor.

If high-resolution data at 100 μm and longer wavelengths were available for a molecular cloud, then one could use those maps to avoid having to subtract the VSG contribution to the observed emission. Unfortunately, the dust temperature and column maps produced by SFD98 using existing 100 and 240 μm data are of much lower resolution ($\sim$1°) than the *IRAS* maps ($\sim$5′). Even nearby molecular clouds require the higher resolution provided

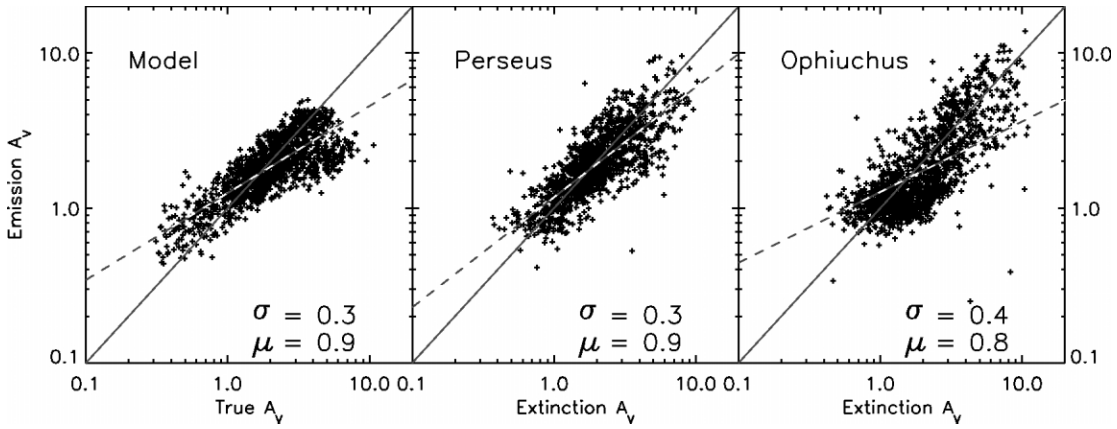

FIG. 3.—Column density derived from 60 and 100 μm emission maps (assuming $\beta = 2$) plotted against the "true" column density. The model's true column density has been altered by Gaussian "noise" with a 1 σ of $0.2A_V$ to match the noise in observational estimates of extinction. The middle and right panels come from Schnee et al. (2005), where the extinction is measured from NIR colors of background stars and the 60 and 100 μm flux from the *IRAS* survey are used to estimate the column density from dust emission. The blue dashed line shows the best fit between the emission-derived column density and the "true" column density. The slope of the model fit is 0.53, which is intermediate between the Perseus and Ophiuchus slopes (0.66 and 0.46, respectively). The values of μ and σ refer to the center and width of the Gaussian fit to the distribution of the ratio ($A_{V_{\rm emission}}/A_{V_{\rm true,\ extinction}}$). [*See the electronic edition of the Journal for a color version of this figure.*]

by *IRAS*, so we compare our model molecular cloud with the observations of Perseus and Ophiuchus using *IRAS* emission maps.

4.4. *Comparison with Observations*

In real molecular clouds, the best estimate of column density often comes from the measured near-infrared (NIR) colors of background stars and is calculated from the reddening done by the intervening dust. Column density maps made this way have a fundamental uncertainty because the background stars have a spread in their intrinsic NIR colors and because the stars included in each pixel of the column density map sample slightly different lines of sight through the molecular cloud. The level of uncertainty is approximately $0.2A_V$, and it is independent of column density (Ridge et al. 2006).

In order to compare our simulation to observations, we have added normally distributed noise (with $1\ \sigma = 0.2$ mag) to the simulated column density. Assuming $\beta = 2$, we then derived the value of X that best matches the emission-derived column density (from the 60 and 100 μm maps) to the new "true" column density. The result is shown in Figure 3.

The left panel of Figure 3 appears similar to the Perseus and Ophiuchus extinction scatter plots, produced as described in Schnee et al. (2005), shown here in the middle and right panels. The emission-based column densities in Perseus and Ophiuchus are derived from *IRAS* 60 and 100 μm maps, and the extinction is derived from NIR color excesses (Ridge et al. 2006). The column derived from FIR emission maps is overestimated at low extinctions and underestimated at high extinctions in both this Letterer and observations. The $1\ \sigma$ width of the Gaussian fit to the ratio of emission-derived column density to absorption-derived column density is 0.3 in our simulation, 0.3 in Perseus, and 0.4 in Ophiuchus, as shown in Figure 3.

We are able to reproduce the scatter observed in Perseus between the column density derived from 60 and 100 μm emission maps and the extinction in our simulation of a turbulent molecular cloud. The dust in our simulation does not have variable emission properties, nor is there a population of transiently heated VSGs. This suggests that neither the variations in dust properties within Perseus nor the emission from VSGs would dominate the uncertainty in the emission-derived column density. Instead, we find that in Perseus, the scatter is primarily explained by the assumption of isothermal dust along each line of sight. In contrast, the Ophiuchus molecular cloud has a larger emission/absorption-derived scatter than can be explained solely by the errors introduced by the assumption of isothermal dust along each line of sight.

We have shown in Schnee et al. (2005) that in order to produce column density maps of nearby molecular clouds from *IRAS* emission maps, it is necessary to determine both the fraction of 60 μm emission that comes from transiently heated dust grains and the conversion factor (X) from 100 μm optical depth to visual extinction, because both of these quantities vary from place to place. These parameters can be determined by the temperature maps of SFD98 and 2MASS/NICER extinction maps.

5. SUMMARY

We have shown that column density estimates from longer wavelength thermal emission maps are less biased and have less uncertainty than estimates made from shorter wavelength maps. In particular, maps of column density derived from 60 and 100 μm emission maps or 100 and 240 μm emission maps systematically overestimate the dust temperature at high extinctions ($>1A_V$ and $4A_V$, respectively) and underestimate the column density.

We have also shown that the observed uncertainty in column density derived from *IRAS* emission maps of Perseus can be fully accounted for by errors introduced by the assumption of isothermal dust along each line of sight through the cloud and uncertainty in the extinction-derived column density. We find no evidence of variable dust emission properties or variations in the fraction of emission at 60 μm from transiently heated VSGs creating significant scatter in column density estimates in Perseus. The observed scatter in the emission/absorption-derived column density in Ophiuchus can be largely, but not fully, explained by the assumption of isothermal dust along each line of sight, suggesting that the VSG emission and/or dust properties vary within the Ophiuchus molecular cloud.

T. Bethell would like to thank Fabian Heitsch for making available his simulations of MHD turbulence. We would like to thank Ellen Zweibel for her numerous insights and helpful suggestions. The 60/100 μm and NIR extinction maps of Perseus and Ophiuchus analyzed in this Letter were created for the COMPLETE Survey of Star-forming Regions (Goodman 2004; Ridge et al. 2006). Scott Schnee is supported under an NSF Graduate Research Fellowship. Tom Bethell is partially supported by NSF AST 03-28821 and NASA ATP 04 0114 to the University of Wisconsin. This work has been partially supported by the National Science Foundation through award AST-0407172.

REFERENCES

Bethell, T., Zweibel, E., Heitsch, F., & Mathis, J. S. 2004, ApJ, 610, 801
Draine, B. T., & Lee, H. M. 1984, ApJ, 285, 89
Dupac, X., et al. 2003, A&A, 404, L11
Goodman, A. A. 2004, in ASP Conf. Ser. 323, Star Formation in the Interstellar Medium: In Honor of David Hollenbach, Chris McKee and Frank Shu, ed. D. Johnstone et al. (San Francisco: ASP), 171
Heitsch, F., Zweibel, E. G., Mac Low, M.-M., Li, P., & Norman, M. 2001, ApJ, 561, 800
Holland, W. S., et al. 1999, MNRAS, 303, 659
Mathis, J. S., Mezger, P. G., & Panagia, N. 1983, A&A, 128, 212
Mathis, J. S., Rumpl, W., & Nordsieck, K. H. 1977, ApJ, 217, 425
Ridge, N., et al. 2006, AJ, in press
Schlegel, D. J., Finkbeiner, D. P., & Davis, M. 1998, ApJ, 500, 525 (SFD98)
Schnee, S. L., Ridge, N. A., Goodman, A. A., & Li, J. G. 2005, ApJ, 634, 442
Stepnik, B., et al. 2003, A&A, 398, 551
Wood, D. O. S., Myers, P. C., & Daugherty, D. A. 1994, ApJS, 95, 457